JCIM JOURNAL OF CHEMICAL INFORMATION AND MODELING

pubs.acs.org/jcim Article

Effects of Defects and Presence of Open-Metal Sites on the Structure and Dynamics of Water in Hydrophobic Zeolitic Imidazolate Frameworks

Yuliang Shi, Dil K. Limbu, Zeyu Zhang, Mohammad R. Momeni,* and Farnaz A. Shakib*

Cite This: J. Chem. Inf. Model. 2023, 63, 7097−7106 Read Online

ACCESS | Metrics & More | Article Recommendations | Supporting Information

ABSTRACT: Most of the chemistry in nanoporous materials with small pore sizes and windows takes place on the outer surface, which is in direct contact with the substrate/solvent, rather than within the pores and channels. Here, we report the results of our comprehensive atomistic molecular dynamics (MD) simulations to decipher the interaction of water with a realistic finite ∼5.1 nm nanoparticle (NP) model of ZIF-8, with edges containing undercoordinated Zn metal sites, vs a conventionally employed pristine crystalline bulk (CB) model. The hydrophobic interior surface of the CB model imparts significant dynamical behavior on water molecules with (i) increasing diffusivity from the surface toward the center of the pores and (ii) confined water, at low concentration, showing similar diffusivity to that of the bulk water. On the other hand, water molecules adsorbed on the surface of the NP model exhibit a range of characteristics, including "coordinated", "confined", and "bulk-like" behavior. Some of the water molecules form coordinative bonds with the undercoordinated Zn metal centers and act as nucleation sites for the water droplets to form, facilitating diffusion into the pores. However, diffusion of water molecules is limited to the areas near the surface and not all the way to the core of the NP model. Our atomistic MD simulations provide insights into the stability of ZIFs in aqueous solutions despite hydrolysis of their outer surface. Such insights are helpful in designing more robust nanoporous materials for applications in humid environments.

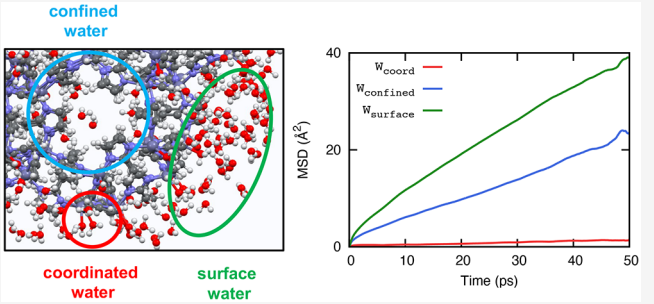

INTRODUCTION

Zeolitic imidazolate frameworks (ZIFs),[1,2] a subclass of metal−organic frameworks (MOFs),[3,4] are chemically tunable permanently porous materials built by forming strong coordinative bonds between tetrahedral Zn and/or Co ions and different imidazolate linkers. Due to their unique structural features, ZIFs have found numerous applications in gas storage,[5] chemical sensing,[6] separation,[7,8] encapsulation and controlled delivery,[9] as well as water harvesting[10,11] and catalysis.[12,13] Zeolite imidazolate framework-8 (ZIF-8), the first member of the ZIF family with 2-methyl imidazolate linkers (Figure 1a), has been the subject of intense research efforts owing to its outstanding physical properties and structural stability,[14−16] with promising breakthrough applications under different environmental conditions. This brings forth the fundamental question of interactions between ZIF-8 and water which, by being present in both atmosphere and aqueous solutions, may significantly influence the structure and hence the properties of the material. Although the hydrophobic nature of ZIF-8 is usually asserted,[17] still the effect of water on the stability of this material is not completely explained or understood. For example, Pan,[18] Zhu,[19] Zhao,[20] and their coworkers reported that ZIF-8 stays structurally stable in boiling water, seawater, and fluoride solutions. On the contrary, Cychosz and Matzger[21] reported degradation of ZIF-8 by immersion in pure water after three months. Afterward, Liu et al.[22] reported that ZIF-8 undergoes hydrolysis when exposed to hydrothermal conditions. Duke et al.[23] found that ZIF-8 shows a significant release of Zn ions, even in deionized water. More recently, experimental reports showed that ZIF-8 nanoparticles (NPs) degrade in humid acidic gases but not under dry acidic gas conditions.[24,25] A more recent work by Taheri and Tsuzuki reported hydrolysis-based decomposition of ZIF-8 in water by the irradiation of UVA, UVB, and near-UV−visible lights, even though ZIF-8 is believed to be inherently photostable.[26]

In the face of such a rather contradictory range of reports, atomistic molecular dynamics (MD) simulations can provide microscopic insights into the competing interatomic water−water vs water−framework interactions and shed light on the structural stability of materials. However, care should be taken

Received: July 14, 2023
Published: October 9, 2023

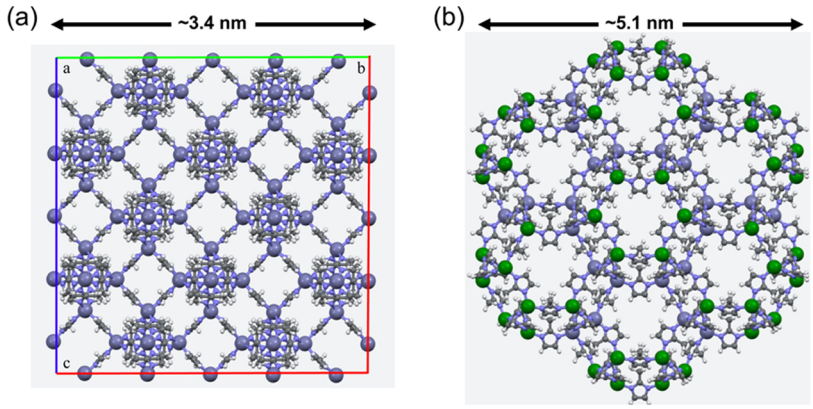

Figure 1. (a) Crystalline bulk (CB) model of ZIF-8 with the sodalite topology, where Zn metal sites are shown with distinctive purple spheres. (b) Finite ∼5.1 nm nanoparticle model of ZIF-8 (3865 atoms) containing coordinatively unsaturated Zn sites on its outer surface (highlighted as green spheres).

in the preparation of model systems for MD simulations. While it has already been shown that some zinc sites on the outer surface of ZIF-8 nanoparticles are undercoordinated,[27] most computational studies to date have focused only on pristine crystalline bulk models where water molecules are confined inside the hydrophobic pores and channels. This approach results in neglecting the effects of the particle's size/shape and external surfaces, which normally contain defects and undercoordinated metal centers. For instance, recently, the structure of 107 °C water vapor inside ZIF-8 was studied by Zhang and co-workers.[28] They did not observe water molecules deforming ZIF-8 and argued that water would stay away from the zinc nodes. Although their conclusions are correct in a crystalline bulk model, they cannot explain the experimental reports on the dissolution of ZIF-8 in water due to the absence of undercoordinated metal centers in their model. For the same reason, when Zhang and Snur used Monte Carlo simulations to simulate the adsorption of water molecules by ZIF-8, they did not find a noticeable interaction between water molecules and metal nodes.[29]

To exploit the predictive power of the computational toolbox and to provide design guidelines for experimental efforts, it is essential to have a molecular-level understanding of how the chosen ZIF model would affect the observed water−framework interactions. Here, we examine the differences in structure and dynamics of water molecules on the inner versus outer surfaces of ZIF-8 using two different models: a 2 × 2 × 2 pristine crystalline bulk (CB) and a finite defective ∼ 5.1 nm nanoparticle (NP) model, which includes edges with undercoordinated open-Zn sites (Figure 1). In total, 50% of Zn sites in the NP model are tricoordinated as opposed to 100% four-coordinated sites in the CB model. Employing all-atom MD simulations, we aim to provide fundamental microscopic molecular-level insights into how water nucleates and grows droplets inside the nanopores and channels of the CB model of ZIF-8 versus on the outer surfaces/edges of the NP model. Our results demonstrate the powerful capability of atomistic MD simulations in providing fundamental mechanistic insights into the interactions of water molecules with ZIF-8 as a representative of hydrophobic materials with small pore sizes and windows.

MODEL AND SIMULATION DETAILS

Atomistic MD simulations were performed on a 2 × 2 × 2 crystalline bulk (CB)[30] and a finite ∼5.1 nm nanoparticle (NP)[31] model of ZIF-8 at 298 K and 1 atm using our in-house software package DL_POLY Quantum v1.0[32] derived from DL_POLY Classic v1.10.[33] The flexible ZIF-FF[34] force field was used for all bonded and nonbonded terms as follows:

$$
\begin{aligned}
E = & \sum_{\text{bonds}} k_r (r - r_0)^2 + \sum_{\text{angles}} k_\theta (\theta - \theta_0)^2 \\
& + \sum_{\text{dihedrals}} k_\phi [1 + \cos(n\phi - \phi_0)] \\
& + \sum_{\text{impropers}} k_\omega [1 + \cos(n\omega - \omega_0)] \\
& + \sum_{\text{Urey-Bradley}} k_u (u - u_0)^2 \\
& + \sum_{\text{nonbonded}} \left(4\epsilon_{ij} \left[\left(\frac{\sigma_{\min_{ij}}}{r_{ij}} \right)^{12} - \left(\frac{\sigma_{\min_{ij}}}{r_{ij}} \right)^{6} \right] + \frac{q_i q_j}{\epsilon_r r_{ij}} \right)
\end{aligned} \tag{1}
$$

In addition to the usual terms, ZIF-FF includes the Urey−Bradley cross-terms with k_u being the force constant and u being the distance between the 1 and 3 atoms. This extra term accounts for the 1,3 nonbonded interactions that are not included in the bond and angle terms. All of the force field parameters are reported in the Supporting Information (SI), Table S1.

The dry CB model was equilibrated for 2 ns in the isothermal−isobaric (NPT) ensemble with a time step of 0.2 fs; see SI Figure S1 for representative convergence plots. An atom−atom cutoff distance of 15.0 Å was employed for truncating the short-range interactions, and the long-range electrostatics were calculated using the Ewald summation method.[35] To build the simulation cell for the NP model, the correct atom types were added to the nanoparticle model obtained from ref 31, which was then placed at the center of a large cubic box of length 120.0 Å to avoid intercell interactions. The atom−atom cutoff distance was set to 35.0 Å. The NP model is positively charged due to the presence of undercoordinated Zn centers on its surface. Therefore, 16 chloride ions were added as counteranions to charge balance the system and arrive at a neutral unit cell. The parameters for the

https://doi.org/10.1021/acs.jcim.3c01077
J. Chem. Inf. Model. 2023, 63, 7097−7106

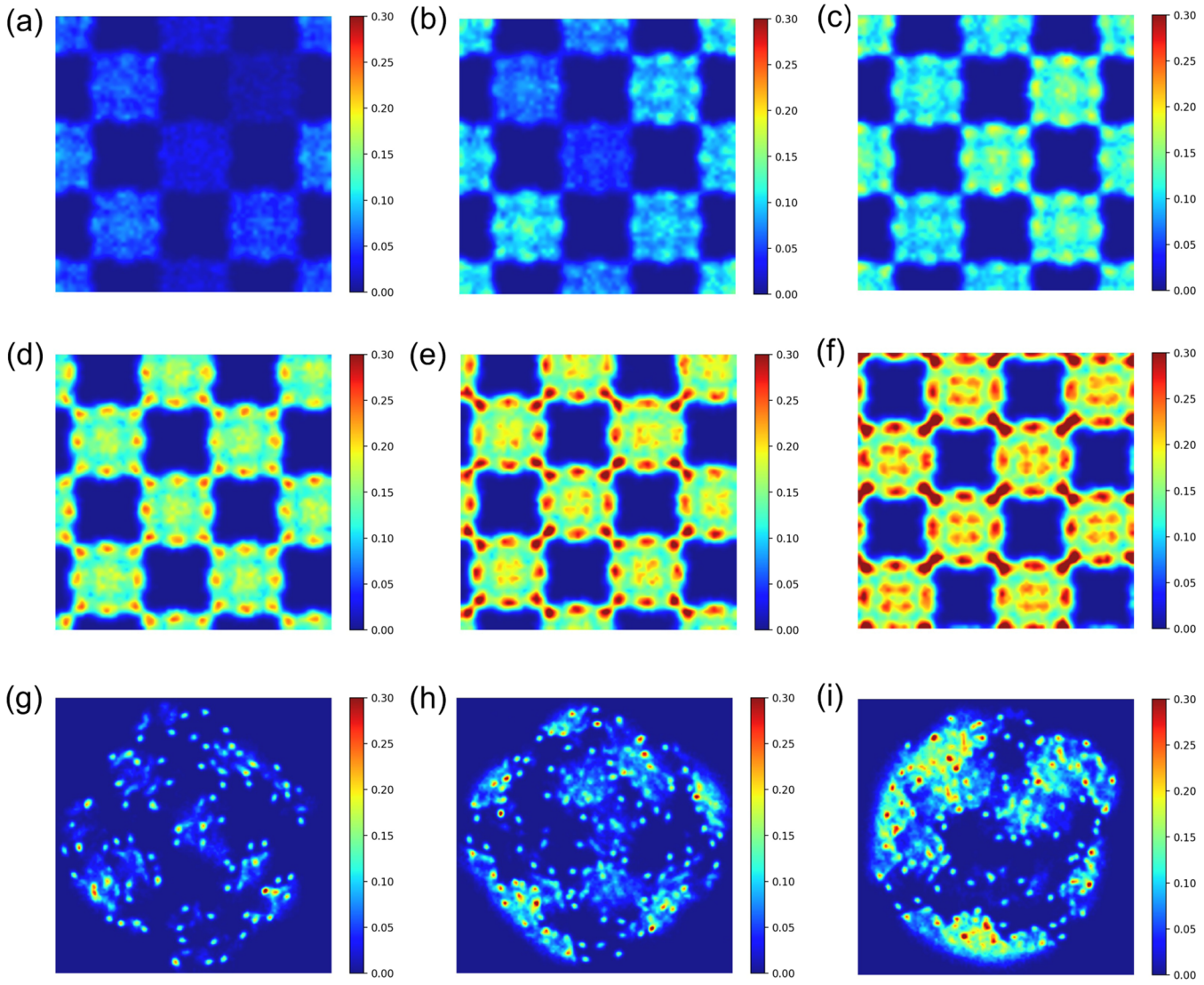

Figure 2. Calculated 2D density maps of the oxygen of water in the CB models with (a) 1n, (b) 2n, (c) 3n, (d) 4n, (e) 5n, and (f) 6n water loadings vs the NP models with (g) 1n, (h) 2n, and (i) 3n water loadings.

chloride ions were taken from ref 36. The counterions were added using PACKMOL[37] in three different configurations, including randomly placed on the outer surface of the NP model as well as placed explicitly on its (100) and (110) faces, as shown in SI Figure S2a. All our systems were equilibrated in the canonical (NVT) ensemble with a time step of 0.5 fs, reaching equilibrium after 2 ns, see SI Figure S3. By inspecting the equilibrated configurations, it was observed that the chloride ions in all three systems stayed only in the outer surface area and did not enter the pores and confined spaces. Figure S2b shows similar configurational energies for the three equilibrated systems. Figure S2c demonstrates Zn−Cl radial distribution functions (RDFs) where Cl ions are coordinated to the tricoordinated Zn centers with similar bond distances in the three systems. Hence, we concluded that the initial position of the chloride counterions would not affect the structure of the ZIF-8 nanoparticle. However, to avoid introducing any bias into our simulations, all three equilibrated systems were used as initial structures in our following simulations for the hydrated systems. In all MD simulations, the equations of motion were propagated according to the velocity−Verlet algorithm. We used the Nosé−Hoover chain (NHC) with four thermostats to keep the temperature constant. In DL_POLY Quantum v1.0, the NHC thermostat is implemented based on the Suzuki−Yoshida scheme for classical simulations in the NVT ensemble,[38−40] whereas the NHC thermostat/barostat for the NPT ensemble is implemented through the Martyna−Tobias−Klein (MTK) algorithm.[41,42] To probe the structure and dynamics of confined water as a function of relative humidity (RH), water molecules were randomly added to the equilibrated dry systems using PACKMOL.[37] 1−6 H_2O per Zn metal centers, hereafter 1n−6n, where n = 96 is the number of Zn centers in the unit cell, were equilibrated in the CB model of ZIF-8. This corresponds to RH of 7.9, 15.8, 23.7, 31.7, 39.6, and 47.5 wt %, respectively, where the RH of 47.5 wt % (maximum of 576 water molecules) represents the saturation limit[28] in the CB model of ZIF-8. For the three NP models, considering the high cost of the simulations due to the size of the nanoparticle and the unit cell, only 1−3 H_2O per Zn metal centers were added to the system (hereafter 1n−3n corresponding to respectively 192, 384, and 576 water molecules). Similar to the dry models, NPT and NVT simulations of 2 ns were found to be sufficient for the equilibration of the hydrated CB and NP models,

https://doi.org/10.1021/acs.jcim.3c01077
J. Chem. Inf. Model. 2023, 63, 7097−7106

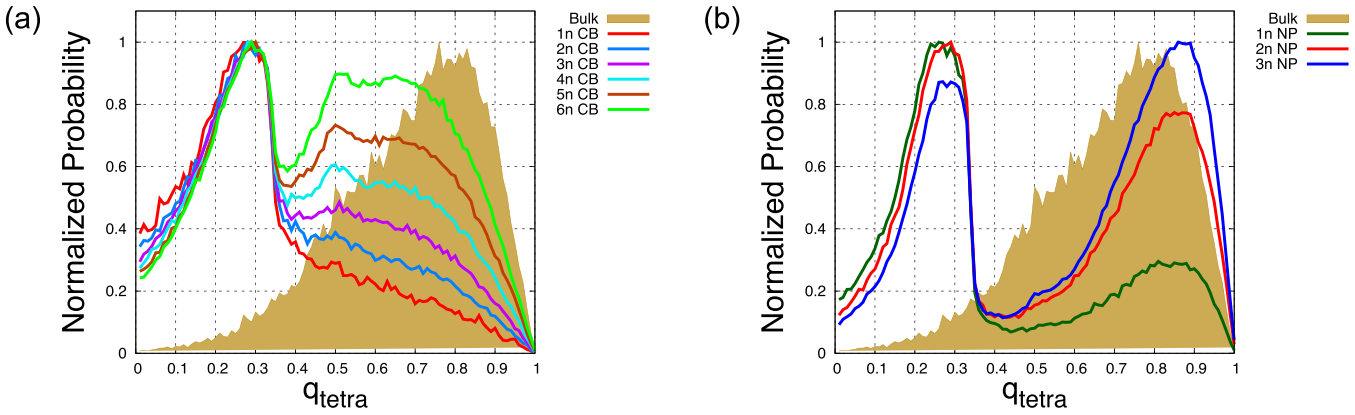

Figure 3. Calculated orientational tetrahedral order parameters for (a) the CB and (b) the NP models of ZIF-8 with different water loadings at 298 K. Corresponding data for bulk water at 298 K are also given for comparison.

respectively (SI Figures S1 and S3). We employed the flexible and anharmonic four-site q-TIP4P/F[43] water potential model as implemented in DL_POLY Quantum v1.0.[32] The framework−water interactions were modeled using the nonbonded electrostatic and Lennard-Jones terms with Lorentz−Berthelot mixing rules used to drive the cross-interaction terms. The appropriateness of the force field parameters used for simulating the interaction of the open-Zn sites with water was established via comparisons to DFT calculations, with details provided in the Supporting Information (SI). Water dynamical properties were calculated from the average of 10 independent 50 ps microcanonical (NVE) trajectories for the CB model while 15 were used for the NP models (5 independent trajectories per each NP model). The initial configurations for the NVE simulations were extracted from a 10 ps NVT simulation of the equilibrated CB and NP models, ensuring the creation of distinctive NVE trajectories.

Recently, Weng and Schmidt have studied the effects of different terminations on slab models of ZIF-8 under a variety of conditions, including temperature, adsorbate pressure, and pH.[44] A combination of DFT and MD data showed that different surface terminations, including Zn, imidazole/imidazolate, and water/hydroxyl, occur depending on the external conditions. However, given the cost of our atomistic simulations, here we assumed that the NP model is only Zn terminated and forms an interface with water molecules through Zn−H_2O bonds. For direct comparisons to experimental data, a more detailed study is warranted in the future that considers different surface terminations including imidazole/imidazolate and OH/OH_2.

RESULTS AND DISCUSSION

Local Structure of Water in CB vs NP Models of ZIF-8.

Figure 2 presents two-dimensional (2D) density maps of water molecules in the CB, Figure 2a−f, and NP, Figure 2g−i, models of ZIF-8 with increasing water loading. These density maps, calculated based on the position of the oxygen of water molecules, provide a qualitative picture of the local structure of water governed by (i) the hydrophobicity of the framework and (ii) the hydrogen bond (HB) network of water molecules. In the CB model, with no undercoordinated open-metal sites, the steric hindrance of the methyl substituents on the imidazolate linkers protects metal centers from the nucleophilic attack of the confined water molecules. Due to the hydrophobic nature of ZIF-8, at low water loadings, low concentrations of water molecules occupy the available vacant spaces of each pore, Figure 2a,b. This is different than a similar hydrophilic material, i.e., ZIF-90, where the centers of the pores are filled only after the surface of the walls is covered with water.[45] However, as the water loading increases, mechanical confinement forces water molecules to diffuse into the nearby pores through narrow channels. This results in a more uniform distribution of water in these confined spaces, which is specifically noticeable in the highest water loadings shown in Figure 2d−f.

As mentioned above, due to the hydrophobicity of the walls in the CB model of ZIF-8, starting from Figure 2c, water molecules create droplets at the center of the pores. At the same time, water molecules are pushed toward the framework due to mechanical confinement and distinct droplets are also formed closer to the surface of the framework. We elect to call these water molecules "interfacial water" as opposed to the ones at the center of the pore, which we elect to call "inner water". As water loading increases, both inner and interfacial water become denser (Figure 2d−f). This organized pattern of water molecules agrees very well with a recent report on the structure of the confined water in the pores of ZIF-8 using the rigid extended simple point charge (SPC/E[46]) model for water and a flexible AMBER adapted force field[47] for ZIF-8.[48] Formation of the interfacial water droplets also leads to confined water molecules forming rather weak hydrogen bonds with the imidazolate nitrogen atoms of the ZIF-8 framework. In the calculated N−H_W radial distribution functions (RDFs), shown in SI Figure S5a, these rather weak interactions appear as a shoulder at ∼3.20 Å as the water content increases.

Figure 2g−i shows 2D density maps for the oxygen of water molecules on the exterior surface of the NP model as water content increases from 1n to 3n. In contrast to the interior surface in the CB model, the exterior surface of the NP model features undercoordinated Zn metal centers (see Figure 1b for the distribution of the open-Zn sites). Hence, water molecules form distinctive coordinative bonds with these open-Zn sites, as evident from the Zn−O_W RDF peaks centered at ∼2.05 Å, see SI Figure S5b. This observation agrees with prior research, which proposed that under sufficiently high water content, water molecules will replace the Zn-bound organic linkers on the ZIF-8 outer surface and form coordinative bonds.[44] Evidently, as the water loading increases, there is a notable tendency for water molecules to aggregate and form large droplets on the surface. This behavior introduces significant

https://doi.org/10.1021/acs.jcim.3c01077
J. Chem. Inf. Model. 2023, 63, 7097−7106

bulk water characteristics into the system. The coordinative water molecules, in the form of $Zn-OH_2$ moieties, are found to act as nucleation sites for the formation of these rather large droplets on the surface of the NP model. Figure S5c demonstrates the $N-H_W$ RDFs for the NP model, which shows rather weak HB interactions with a shoulder appearing around ~2.5 Å as water content increases. This is shorter than the distance of ~3.20 Å in the CB model indicating a stronger interaction, even though still rather weak in nature. Interestingly, examining the equilibrated systems shows that several water molecules start to diffuse into the NP model; we will discuss this in more detail in the next sections.

Order Parameter and Local Structure of Water. To shed more light on the local structure and HB network of water in different studied ZIF-8 models, we calculated the normalized orientational tetrahedral order parameter (q_{tetra}),[49−51] which identifies the presence of four nearest neighbor water oxygen atoms according to

$$q_{tetra} = 1 - \frac{3}{8}\sum_{j=1}^{3}\sum_{k=j+1}^{4}\left(\cos\psi_{jk} + \frac{1}{3}\right)^2 \quad (2)$$

here, ψ_{jk} is the angle formed between the oxygen atom of the water of interest and its nearest neighbor oxygen atoms (j) and (k) (located at distances less than 3.5 Å). The q_{tetra} values range from 0 for an ideal gas to 1, which indicates an icelike structure with a close-to-perfect tetrahedral arrangement. Figure 3 illustrates our MD calculated q_{tetra} values for the 1n−6n water loading in the CB model (Figure 3a) vs 1n−3n water loading in the NP model (Figure 3b). A reference peak for the simulated bulk water, a filled yellow peak, is also included for comparison. For both models, sharp peaks centered at $q_{tetra} \sim 0.28$ can be found in all water loadings related to the interfacial water regardless of the interior or exterior surface. This reduced order is observed because the interfacial water molecules form hydrogen bonds with the neighboring water molecules from one side while the other side is restricted by the inner or outer surface of the framework. Hence, they demonstrate distinctive arrangements compared to the bulk water.

As water content increases from 1n to 6n in the CB model, a broader peak emerges in the $q_{tetra} \sim 0.4-0.8$. The overlap with the reference bulk peak signals the formation of water droplets in agreement with our calculated 2D density maps as discussed before (Figure 2). Despite the growing overlap with the bulk water peak as the water loading increases, these broad peaks are still related to the confined water in the pores of the CB model. Hence, generally, they all are less ordered than bulk water. Our findings regarding the contributions to these two peaks closely parallel the conclusions drawn in a prior study that investigated the hydrogen bond structure of confined water, employing a MOF featuring open-metal sites.[52] While the interfacial water peaks at $q_{tetra} \sim 0.28$ in the NP model (Figure 3b) resemble those observed for the CB model, the bulk-like behavior is slightly different. The peak around $q_{tetra} \sim 0.5$ almost vanishes while another peak at $q_{tetra} \sim 0.85$ dominates. As expected, this shows the high affinity of water molecules to form an intermolecular water−water HB network when they are not restricted by mechanical confinement. As the water content increases, the bulk-like peak starts to grow taller than the interfacial water peak, which mirrors the increasing size of the droplets.

Characterizing Diverse Dynamical Features of Water in Different ZIF-8 Models. The qualitative picture of water structure and distribution within the pores of the CB model and the surface of the NP models indicates the presence of different classes of water molecules in both systems. To provide a quantitative picture, we differentiate these classes by calculating their dynamical properties, including reorientation relaxation time (τ_2) and total self-diffusivity (D_{tot}). We calculate D_{tot} based on the mean square displacement (MSD) of water molecules as follows:

$$D_{tot} = \lim_{t\to+\infty}\frac{1}{6t}\langle\{r(t) - r(0)\}^2\rangle \quad (3)$$

To quantify τ_2, we calculated orientational time correlation functions (TCFs). These TCFs are formulated based on the reorientation of the unit vector $\hat{\mathbf{u}}_{OH}$, which represents the orientation of one of the OH bonds in a water molecule. Accordingly, we have

$$C_{2,OH}(t) = \langle P_2[\hat{u}_{OH}(0)\hat{u}_{OH}(t)]\rangle \quad (4)$$

where P_2 is the Legendre polynomial of order 2. In order to determine τ_2 values, a fitting analysis was performed on the ensemble-averaged correlation functions obtained from all water molecules (in the selected regions) over time. The correlation functions were then fitted to a biexponential function in the following form:

$$C_{2,OH}(t) = \left[a \times \exp\left(-\frac{t}{\tau_1}\right)\right] + \left[b \times \exp\left(-\frac{t}{\tau_2}\right)\right] \quad (5)$$

The final reorientation relaxation times were finally calculated from the weighted average of the fitting parameters:

$$\tau_{reor} = \frac{(a \times \tau_1) + (b \times \tau_2)}{(a + b)} \quad (6)$$

We divide the spherical central pore of the CB model into two concentric regions, as shown in Figure 4, to represent the

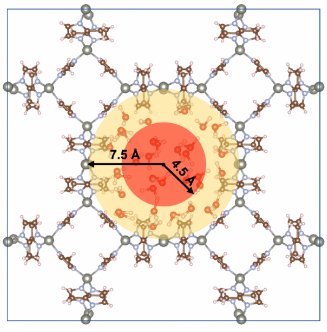

Water type	ZIF-8 (CB) τ_2	ZIF-8 (CB) D_{tot}
W_{inner}	5.0±0.7	0.071±0.005
$W_{interfacial}$	10.7±1.3	0.052±0.004
Simul. bulk water	2.8±0.6	0.193±0.018
Exp. bulk water	1.7−2.6[53−55]	0.229[56]

Figure 4. Inner (red) vs interfacial (yellow) regions of the confined water in the CB model of ZIF-8 with the highest 6n water loading. The table shows differences in the computed τ_2 (in ps) and D_{tot} (in Å²/ps) values between the two regions. The corresponding $C_2(t)$ and MSD (Å²) plots are given in SI Figure S5a,b. Water molecules present in the nearby pores have been omitted for clarity.

https://doi.org/10.1021/acs.jcim.3c01077
J. Chem. Inf. Model. 2023, 63, 7097−7106

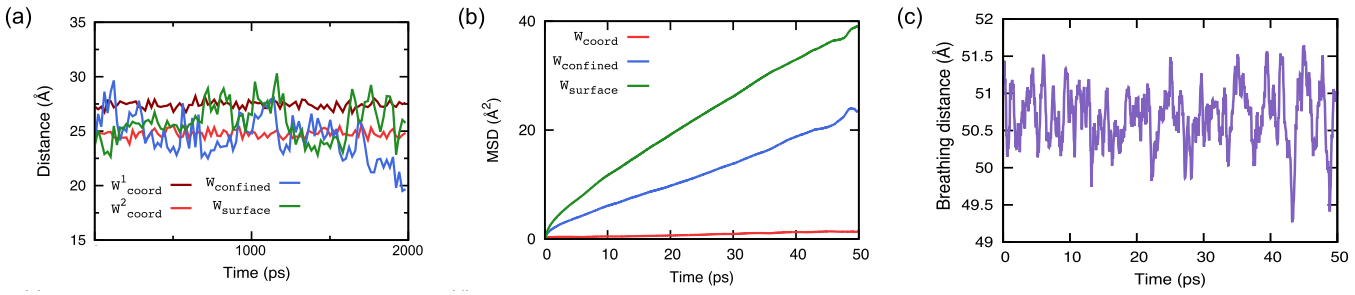

Figure 5. (a) Representative NVT trajectories highlighting different classes of water molecules present in the hydrated NP model with 3n water loading; the *y*-axis represents the distance of the center of mass (CoM) of the representative water molecules from the CoM of the NP model (for all water molecules see SI Figure S8). (b) Calculated MSD (Å^2) values for different water types from the NVE simulations. (c) Breathing of the NP model; the *y*-axis represents the distance between two Zn centers on opposite ends.

"inner" and "interfacial" water introduced in the previous section. The radius of the inner region (shown in red) is chosen to be 4.5 Å, while the radius of the outer region (shown in yellow) is adapted to be larger than 4.5 Å and smaller than 7.5 Å. The highest 6n water loading, which corresponds to a relative humidity of ∼47.5 wt % and the saturation limit in the CB model of ZIF-8,[28] is employed to highlight the differences in the calculated dynamical properties of water in these two regions. The embedded table in Figure 4 shows the calculated average τ_2 and D_{tot} values in the two regions among 12 intact pores in the 2 × 2 × 2 unit cell. The corresponding experimental and simulated data for bulk water are also given for comparison. For simulating bulk water, 216 water molecules were packed inside a cubic box of length 35.233 au corresponding to a density of 0.997 g/cm^3 at 298 K with the atom−atom cutoff distance set to 9.0 Å. The small values of D_{tot} in both regions of the CB model compared to bulk water indicate the overall low mobility of water molecules due to the mechanical confinement effects in ZIF-8. However, a comparison between both τ_2 and D_{tot} values clearly shows that water molecules are rendered less mobile as they get closer to the surface of hydrophobic ZIF-8. In other words, inner water molecules are more mobile since their movement is not restricted by methyl substituents that have decorated the interior walls of the ZIF-8.

Water in the NP model has a structure that is rather more complex than that in the CB model. It can be classified into four representative categories as displayed in Figure 5a based on the distances of the centers of mass (CoM) of the water molecules from the CoM of the NP model. W_{coord}^1 and W_{coord}^2 represent water molecules coordinated to the open-metal sites on the surface of the nanoparticle pointing toward either its exterior or its interior, respectively. As seen from Figure 5a, the movement of these coordinated water molecules is limited. It can be inferred from this plot that coordination occurs in the very early stages of the simulation and remains stable until the end of the equilibration. $W_{confined}$ represents water molecules with a very vivid range of motions that are finally able to diffuse into the NP. In contrast, $W_{surface}$ represents "surface" water molecules that stay around the surface of the NP model, despite their vivid motions. They mostly belong to the water droplets that grow outward the surface of the nanoparticle. From now on, we group W_{coord}^1 and W_{coord}^2 together, as they are not expected to differ in their dynamical behavior. Figure 5b highlights the differences in the dynamical behavior of three classes of water molecules in the NP model in the context of the MSD plots for the highest studied 3n water loading averaged over 15 NVE trajectories. While the coordinated water is almost fixed in place, the other two classes have a mobile nature, though the surface water naturally has more freedom of movement than the confined water. The D_{tot} values extracted from these plots are presented in Table 1 which confirm the highest mobility for the surface water, i.e., 0.147 vs 0.079 Å^2/ps for the confined water. While the calculated D_{tot} value for W_{coord} is very low, i.e., 0.011 Å^2/ps, it is still not zero. The reason partially can be traced back to the breathing motions of the ZIF-8 nanoparticle. Figure 5c shows the change in average distances between the two Zn metal sites on two opposing ends of the NP model during our NVE simulations, which shows a contraction/expansion rhythm. In short, despite the coordinated nature of W_{coord}, it moves alongside the NP model as it contracts and shrinks. Hence, it is not surprising that the calculated τ_2 value for W_{coord} is not that much higher than $W_{confined}$, 19.8 vs 16.5 ps. Still, both values are considerably higher than the 4.7 ps calculated for $W_{surface}$.

Table 1. Computed Water Reorientation Relaxation Time (τ_2 in ps) and Total Self-Diffusivity (D_{tot} in Å^2/ps) for the CB and NP Models of ZIF-8 with Different Water Loadings[a]

	ZIF-8 (CB)		
water loading	τ_2	D_{tot}	ΔH_{ads}
1n	2.7 ± 0.6	0.195 ± 0.017	−1.2
2n	3.3 ± 0.6	0.168 ± 0.014	−1.5
3n	4.3 ± 0.7	0.136 ± 0.013	−2.3
4n	4.6 ± 0.7	0.121 ± 0.007	−3.0
5n	6.6 ± 0.8	0.088 ± 0.005	−3.2
6n	8.5 ± 0.9	0.061 ± 0.004	−3.7
	ZIF-8 (NP)		
water loading	τ_2	D_{tot}	ΔH_{ads}
1n	14.6 ± 1.4	0.070 ± 0.004	−12.6
2n	9.1 ± 1.1	0.112 ± 0.007	−11.7
3n	8.6 ± 1.0	0.133 ± 0.012	−10.7

[a]The corresponding MD simulated (simul.) and experimental (experimental) values for bulk water at 298 K are also given for comparison. The corresponding orientational time correlation function (C_2, t) and mean square displacement (MSD, Å^2) plots are given in SI Figure S7. The enthalpy of adsorption (ΔH_{ads} in kcal/mol) for different systems is also given.

Average Thermodynamic/Dynamical Properties of Water in Different ZIF-8 Models. Table 1 summarizes the calculated relaxation times and diffusion coefficients, as well as

https://doi.org/10.1021/acs.jcim.3c01077
J. Chem. Inf. Model. 2023, 63, 7097−7106

enthalpy of adsorption per water molecule (ΔH_{ads}) for all studied water loadings for both the CB and the NP models of ZIF-8. All water molecules from any type and region are included in these calculations. We note that one reaches the saturation limit in the 6n loading for the CB model; however, the same does not apply to the NP model due to computational limitations. Still, it is interesting to have an average quantitative picture of water thermodynamics/dynamical properties in the NP model.

We calculated ΔH_{ads} as follows:

$$\Delta H_{ads} = \frac{1}{n}[H_{n@ZIF} - H_{ZIF} - (n \times H_{wat})] \quad (7)$$

where H_{MOF} and $H_{n@MOF}$ refer to the enthalpy of the dry and hydrated ZIF-8 models with n being the number of water molecules. H_{wat} is the enthalpy of a single q-TIP4P/F water molecule. In the CB model, the hydrophobic interior walls of ZIF-8 with all saturated Zn sites impart up to 10 times smaller ΔH_{ads} values compared to the NP model. As mentioned above, confined water molecules form only weak HBs with the imidazolate nitrogen atoms in the CB model. Overall, the calculated ΔH_{ads} values for the CB model of ZIF-8 show a linearly augmenting water−framework interaction as water content increases. On the other hand, for the NP model, water molecules form rather strong coordinative bonds with the open-Zn sites which contributes to the more negative ΔH_{ads} values (−10.7 to −12.6 kcal/mol). As the water content in the NP model increases, the adsorption enthalpy becomes less negative. This can be attributed to the fact that the limited number of open-Zn sites present on the surface of the NP model is already saturated for the 1n water loading. However, as explained above, since our studied water contents for the NP model do not reach the saturation limit, caution should be taken in generalizing the computed average values.

For the CB model with no undercoordinated open-metal sites, calculated τ_2 values increase exponentially with water loading while D_{tot} shows a linear decrease. This is primarily due to the mechanical confinement effects and the fact that as the loading increases, water molecules are forced to move closer to the surface of the hydrophobic ZIF-8 where their mobility becomes even more limited compared to the center of the pore. Interestingly, a closer look at the computed τ_2 and D_{tot} values of the lowest 1n water content, which corresponds to a relative humidity of ∼8 wt %, reveals dynamical behavior similar to that observed for bulk water (see embedded table in Figure 4). This rather high mobility of a relatively low water concentration in hydrophobic ZIF-8 agrees qualitatively well with a recent study on water transport in hydrophobic hBN nano-capillaries where monolayer water clusters were shown to have diffusion coefficients up to 4 times higher than that of bulk water.[57] Our findings in this work are also generally in accordance with previous studies on the anomalous behavior of water at extreme mechanical nano/subnanoconfinement conditions.[58−64] This phenomenon is also similar to what has already been shown for proton transport in small linear water wires[65] and in narrow channels of the (6,6) carbon nanotubes.[66] This could be translated to overall lower barriers for proton/electron transfer or proton-coupled electron-transfer reactions in hydrophobic nanoconfinements which can open up new opportunities, for example, in designing super ion conducting polymeric channels.[61−64]

In contrast to what was observed in the CB model, the computed τ_2 value for the 1n water loading in the NP model is relatively high, pointing to the localization of water molecules on the surface of the NP model due to coordination to the open-metal sites (Figure 6). The increase in water loading

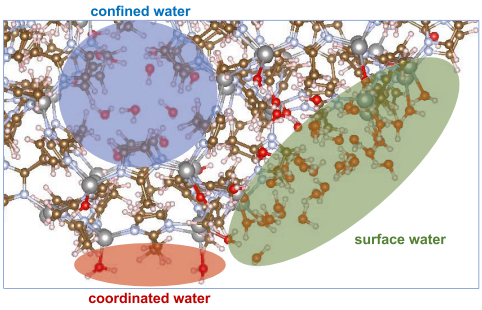

Water types	ZIF-8 (NP) τ_2	ZIF-8 (NP) D_{tot}
$W_{surface}$	4.7±0.7	0.147±0.013
$W_{confined}$	16.5±1.5	0.079±0.005
W_{coord}	19.8±1.9	0.011±0.001

Figure 6. Surface water (green) vs confined water (blue) vs coordinated water (red) in the NP model of ZIF-8 with the highest 6n water loading. The table shows differences in the computed τ_2 (in ps) and D_{tot} (in Å^2/ps) values between the three types. The corresponding $C_2(t)$ plot is given in SI Figure S5c.

leads to the creation of larger droplets with more bulk-like character, resulting in a decrease in τ_2 and an increase in D_{tot} values. We further analyzed the dynamics of each individual water molecule by tracking its distance from the CoM of the NP model. The results are shown in SI Figure S8, which demonstrate that the density of water molecules diffusing into the nanoparticle as well as their diffusion range increases significantly with increasing water content, despite the hydrophobic nature of the interior walls of the framework. At the same time, water molecules are never able to reach the CoM of the NP and instead tend to stay closer to the surface. These observations qualitatively agree with the available experimental data[25] that hydrolysis was observed to only occur on the surface of ZIF-8 and was found not to affect its core. This is most likely due to a combination of the small pore sizes and windows of ZIF-8 along with the highly hydrophobic nature of its interior walls.

Overall, the rather significant differences observed in calculated structural and dynamical properties of water in the CB vs the NP models of ZIF-8, as a representative of hydrophobic nanoporous materials, underscore the importance of adapting suitable models for simulating these materials especially if comparisons to experimental data are desired.

CONCLUSIONS

Differentiating between a pristine crystalline bulk (CB) model of ZIF-8, conventionally used in computational studies, and a nanoparticle (NP) model, representing a realistic system containing defects and edges with undercoordinated metal sites, we investigated water structure and dynamics using atomistic MD simulations. Rather significant differences in structure and dynamical properties of water were observed with two classes of confined water being found for the CB model, whereas three different classes were identified for water in the NP model. The combination of adopting a suitable model system and carefully carrying out atomistic MD simulations with flexible potentials for both the framework

https://doi.org/10.1021/acs.jcim.3c01077
J. Chem. Inf. Model. 2023, 63, 7097−7106

and water can lead to theories with more predictable power and bring atomistic MD one step closer to the experiment. Future works should be directed toward the spectroscopic characterization of different classes of water molecules as well as probing the effects of incorporating nuclear quantum effects in simulating the structural and dynamical properties of water.

■ ASSOCIATED CONTENT

Data Availability Statement

Our in-house developed DL_POLY Quantum software v1.0 used for carrying out MD simulations in this work is available through our GitHub repository at https://github.com/fashakib/DL_POLY-Quantum-v1.0. Interested users can consult with example cases that are provided for different systems in the "data" subdirectory. The input and output files of MD simulations in this work are provided as part of the Supporting Information.

Supporting Information

The Supporting Information is available free of charge at https://pubs.acs.org/doi/10.1021/acs.jcim.3c01077.

ZIF-FF force field parameters; E, T, and P plots of equilibrated systems; radial distribution functions; orientational time correlation functions; mean square displacements; and details of our DFT calculations (PDF)

Input and output files of the MD simulations (ZIP)

■ AUTHOR INFORMATION

Corresponding Authors

Mohammad R. Momeni − *Division of Energy, Matter and Systems, School of Science and Engineering, University of Missouri—Kansas City, Kansas City, Missouri 64110, United States;* orcid.org/0000-0002-7731-5823; Email: mmomenitaheri@umkc.edu

Farnaz A. Shakib − *Department of Chemistry and Environmental Science, New Jersey Institute of Technology, Newark, New Jersey 07102, United States;* orcid.org/0000-0003-1432-2812; Email: shakib@njit.edu

Authors

Yuliang Shi − *Department of Chemistry and Environmental Science, New Jersey Institute of Technology, Newark, New Jersey 07102, United States*

Dil K. Limbu − *Department of Chemistry and Environmental Science, New Jersey Institute of Technology, Newark, New Jersey 07102, United States;* orcid.org/0000-0001-9196-9498

Zeyu Zhang − *Department of Chemistry and Environmental Science, New Jersey Institute of Technology, Newark, New Jersey 07102, United States*

Complete contact information is available at: https://pubs.acs.org/10.1021/acs.jcim.3c01077

Notes

The authors declare no competing financial interest.

■ ACKNOWLEDGMENTS

This research was supported by the National Science Foundation through grant nos. CBET-2302617 and CBET-2302618. This work used resources from Bridges2 at Pittsburgh Supercomputing Center through allocations CHE200007, CHE200008, and PHY230099 from the Extreme Science and Engineering Discovery Environment (XSEDE),[67] which was supported by National Science Foundation grant number 1548562.

■ REFERENCES

(1) Huang, X.-C.; Lin, Y.-Y.; Zhang, J.-P.; Chen, X.-M. Ligand-Directed Strategy for Zeolite-Type Metal-Organic Frameworks: Zinc(II) Imidazolates with Unusual Zeolitic Topologies. *Angew. Chem., Int. Ed.* **2006**, *45*, 1557−1559.

(2) Park, K. S.; Ni, Z.; Côté, A. P.; Choi, J. Y.; Huang, R.; Uribe-Romo, F. J.; Chae, H. K.; O'Keeffe, M.; Yaghi, O. M. Exceptional chemical and thermal stability of zeolitic imidazolate frameworks. *Proc. Natl. Acad. Sci. U.S.A.* **2006**, *103*, 10186−10191.

(3) Furukawa, H.; Cordova, K. E.; OKeeffe, M.; Yaghi, O. M. The Chemistry and Applications of Metal-Organic Frameworks. *Science* **2013**, *341*, No. 1230444.

(4) Yaghi, O. M.; O'Keeffe, M.; Ockwig, N. W.; Chae, H. K.; Eddaoudi, M.; Kim, J. *Nature* **2003**, *423*, 705−714.

(5) Banerjee, R.; Phan, A.; Wang, B.; Knobler, C.; Furukawa, H.; O'Keeffe, M.; Yaghi, O. M. High-Throughput Synthesis of Zeolitic Imidazolate Frameworks and Application to CO_2 Capture. *Science* **2008**, *319*, 939−943.

(6) Lu, G.; Hupp, J. T. Metal-Organic Frameworks as Sensors: A ZIF-8 Based Fabry-Perot Device as a Selective Sensor for Chemical Vapors and Gases. *J. Am. Chem. Soc.* **2010**, *132*, 7832−7833.

(7) Li, K.; Olson, D. H.; Seidel, J.; Emge, T. J.; Gong, H.; Zeng, H.; Li, J. Zeolitic Imidazolate Frameworks for Kinetic Separation of Propane and Propene. *J. Am. Chem. Soc.* **2009**, *131*, 10368−10369.

(8) Chang, N.; Gu, Z.-Y.; Yan, X.-P. Zeolitic Imidazolate Framework-8 Nanocrystal Coated Capillary for Molecular Sieving of Branched Alkanes from Linear Alkanes along with High-Resolution Chromatographic Separation of Linear Alkanes. *J. Am. Chem. Soc.* **2010**, *132*, 13645−13647.

(9) Liédana, N.; Galve, A.; Rubio, C.; Téllez, C.; Coronas, J. CAF@ZIF-8: One-Step Encapsulation of Caffeine in MOF. *ACS Appl. Mater. Interfaces* **2012**, *4*, 5016−5021.

(10) Kim, H.; Yang, S.; Rao, S. R.; Narayanan, S.; Kapustin, E. A.; Furukawa, H.; Umans, A. S.; Yaghi, O. M.; Wang, E. N. Water harvesting from air with metal-organic frameworks powered by natural sunlight. *Science* **2017**, *356*, 430−434.

(11) Hanikel, N.; Prévot, M. S.; Fathieh, F.; Kapustin, E. A.; Lyu, H.; Wang, H.; Diercks, N. J.; Glover, T. G.; Yaghi, O. M. Rapid Cycling and Exceptional Yield in a Metal-Organic Framework Water Harvester. *ACS Cent. Sci.* **2019**, *5*, 1699−1706.

(12) Chen, B.; Yang, Z.; Zhu, Y.; Xia, Y. Zeolitic imidazolate framework materials: recent progress in synthesis and applications. *J. Mater. Chem. A* **2014**, *2*, 16811−16831.

(13) Cheng, N.; Ren, L.; Xu, X.; Du, Y.; Dou, S. X. Recent Development of Zeolitic Imidazolate Frameworks (ZIFs) Derived Porous Carbon Based Materials as Electrocatalysts. *Adv. Energy Mater.* **2018**, *8*, No. 1801257.

(14) Bhattacharyya, S.; Pang, S. H.; Dutzer, M. R.; Lively, R. P.; Walton, K. S.; Sholl, D. S.; Nair, S. Interactions of SO_2-Containing Acid Gases with ZIF-8: Structural Changes and Mechanistic Investigations. *J. Phys. Chem. C* **2016**, *120*, 27221−27229.

(15) Bergaoui, M.; Khalfaoui, M.; Awadallah-F, A.; Al-Muhtaseb, S. A review of the features and applications of ZIF-8 and its derivatives for separating CO_2 and isomers of C_3- and C_4- hydrocarbons. *J. Nat. Gas Sci. Eng.* **2021**, *96*, No. 104289.

(16) Leus, K.; Bogaerts, T.; De Decker, J.; Depauw, H.; Hendrickx, K.; Vrielinck, H.; Van Speybroeck, V.; Van Der Voort, P. ystematic study of the chemical and hydrothermal stability of selected "stable" Metal Organic Frameworks. *Microporous Mesoporous Mater.* **2016**, *226*, 110−116.

(17) Ortiz, A. U.; Freitas, A. P.; Boutin, A.; Fuchs, A. H.; Coudert, F.-X. What makes zeolitic imidazolate frameworks hydrophobic or hydrophilic? The impact of geometry and functionalization on water adsorption. *Phys. Chem. Chem. Phys.* **2014**, *16*, 9940−9949.

(18) Pan, Y.; Liu, Y.; Zeng, G.; Zhao, L.; Lai, Z. Rapid synthesis of zeolitic imidazolate framework-8 (ZIF-8) nanocrystals in an aqueous system. *Chem. Commun.* **2011**, *47*, 2071−2073.
(19) Zhu, Y.; Gupta, K. M.; Liu, Q.; Jiang, J.; Caro, J.; Huang, A. Synthesis and seawater desalination of molecular sieving zeolitic imidazolate framework membranes. *Desalination* **2016**, *385*, 75−82.
(20) Zhao, X.; Liu, D.; Huang, H.; Zhang, W.; Yang, Q.; Zhong, C. The stability and defluoridation performance of MOFs in fluoride solutions. *Microporous Mesoporous Mater.* **2014**, *185*, 72−78.
(21) Cychosz, K. A.; Matzger, A. J. Water Stability of Microporous Coordination Polymers and the Adsorption of Pharmaceuticals from Water. *Langmuir* **2010**, *26*, 17198−17202.
(22) Liu, X.; Li, Y.; Ban, Y.; Peng, Y.; Jin, H.; Bux, H.; Xu, L.; Caro, J.; Yang, W. Improvement of hydrothermal stability of zeolitic imidazolate frameworks. *Chem. Commun.* **2013**, *49*, 9140−9142.
(23) Duke, M. C.; Zhu, B.; Doherty, C. M.; Hill, M. R.; Hill, A. J.; Carreon, M. A. Structural effects on SAPO-34 and ZIF-8 materials exposed to seawater solutions, and their potential as desalination membranes. *Desalination* **2016**, *377*, 128−137.
(24) Bhattacharyya, S.; Han, R.; Kim, W.-G.; Chiang, Y.; Jayachandrababu, K. C.; Hungerford, J. T.; Dutzer, M. R.; Ma, C.; Walton, K. S.; Sholl, D. S.; Nair, S. Acid Gas Stability of Zeolitic Imidazolate Frameworks: Generalized Kinetic and Thermodynamic Characteristics. *Chem. Mater.* **2018**, *30*, 4089−4101.
(25) Pang, S. H.; Han, C.; Sholl, D. S.; Jones, C. W.; Lively, R. P. Facet-Specific Stability of ZIF-8 in the Presence of Acid Gases Dissolved in Aqueous Solutions. *Chem. Mater.* **2016**, *28*, 6960−6967.
(26) Taheri, M.; Tsuzuki, T. Photo-accelerated Hydrolysis of Metal Organic Framework ZIF-8. ACS. *Mater. Lett.* **2021**, *3*, 255−260.
(27) Chizallet, C.; Lazare, S.; Bazer-Bachi, D.; et al. Catalysis of Transesterification by a Nonfunctionalized Metal-Organic Framework: Acido-Basicity at the External Surface of ZIF-8 Probed by FTIR and ab Initio Calculations. *J. Am. Chem. Soc.* **2010**, *132*, 12365−12377.
(28) Zhang, L.; Zheng, B.; Gao, Y.; Wang, L.; Wang, J.; Duan, X. Confined Water Vapor in ZIF-8 Nanopores. *ACS Omega* **2022**, *7*, 64−69.
(29) Zhang, H.; Snurr, R. Q. Computational Study of Water Adsorption in the Hydrophobic Metal-Organic Framework ZIF-8: Adsorption Mechanism and Acceleration of the Simulations. *J. Phys. Chem. C* **2017**, *121*, 24000−24010.
(30) Lewis, D. W.; Ruiz-Salvador, A. R.; Gómez, A.; Rodriguez-Albelo, L. M.; Coudert, F.-X.; Slater, B.; Cheetham, A. K.; Mellot-Draznieks, C. Zeolitic imidazole frameworks: structural and energetics trends compared with their zeolite analogues. *CrystEngComm* **2009**, *11*, 2272−2276.
(31) Proenza, Y. G.; Longo, R. L. Simulation of the Adsorption and Release of Large Drugs by ZIF-8. *J. Chem. Inf. Model.* **2020**, *60*, 644−652.
(32) Momeni, M. R.; Shakib, F. A. The DL_POLY Quantum Molecular Simulation Package, 2023. https://github.com/fashakib/DL_POLY-Quantum-v1.0.
(33) Smith, W.; Forester, T. R.; Todorov, I. T. STFC Daresbury Laboratory. The DL_POLY Classic Molecular Simulation Package, 2023. https://gitlab.com/DL_POLY_Classic.
(34) Weng, T.; Schmidt, J. R. Flexible and Transferable ab Initio Force Field for Zeolitic Imidazolate Frameworks: ZIF-FF. *J. Phys. Chem. A* **2019**, *123*, 3000−3012.
(35) Leach, A. R. *Molecular Modeling: Principles and Applications*; Pearson Prentice Hall, 2001.
(36) Zeron, I. M.; Abascal, J. L. F.; Vega, C. A force field of Li^+, Na., K^+, Mg^{2+}, Ca^{2+}, Cl^-, and SO_4^{2-} in aqueous solution based on the TIP4P/2005 water model and scaled charges for the ions. *J. Chem. Phys.* **2019**, *151*, No. 134504.
(37) Martínez, L.; Andrade, R.; Birgin, E. G.; Martínez, J. M. PACKMOL: A package for building initial configurations for molecular dynamics simulations. *J. Comput. Chem.* **2009**, *30*, 2157−2164.
(38) Yoshida, H. Construction of higher order symplectic integrators. *Phys. Lett. A* **1990**, *150*, 262−268.
(39) Suzuki, M. General theory of fractal path integrals with applications to many-body theories and statistical physics. *J. Math. Phys.* **1991**, *32*, 400−407.
(40) Martyna, G. J.; Tuckerman, M. E.; Tobias, D. J.; Klein, M. L. Explicit reversible integrators for extended systems dynamics. *Mol. Phys.* **1996**, *87*, 1117−1157.
(41) Martyna, G. J.; Tobias, D. J.; Klein, M. L. Constant pressure molecular dynamics algorithms. *J. Chem. Phys.* **1994**, *101*, 4177−4189.
(42) Tuckerman, M. E.; Alejandre, J.; López-Rendón, R.; Jochim, A. L.; Martyna, G. J. A Liouville-operator derived measure-preserving integrator for molecular dynamics simulations in the isothermal−isobaric ensemble. *J. Phys. A: Math. Gen.* **2006**, *39*, 5629−5651.
(43) Habershon, S.; Markland, T. E.; Manolopoulos, D. E. Competing quantum effects in the dynamics of a flexible water model. *J. Chem. Phys.* **2009**, *131*, No. 024501.
(44) Weng, T.; Schmidt, J. R. Structure and Thermodynamic Stability of Zeolitic Imidazolate Framework Surfaces. *J. Phys. Chem. C* **2020**, *124*, 1458−1468.
(45) Wagner, J. C.; Hunter, K. M.; Paesani, F.; Xiong, W. Water Capture Mechanisms at Zeolitic Imidazolate Framework Interfaces. *J. Am. Chem. Soc.* **2021**, *143*, 21189−21194.
(46) Berendsen, H. J. C.; Grigera, J. R.; Straatsma, T. P. The missing term in effective pair potentials. *J. Phys. Chem. A* **1987**, *91*, 6269−6271.
(47) Zheng, B.; Sant, M.; Demontis, P.; Suffritti, G. B. Force Field for Molecular Dynamics Computations in Flexible ZIF-8 Framework. *J. Phys. Chem. C* **2012**, *116*, 933−938.
(48) Fraux, G.; Boutin, A.; Fuchs, A. H.; Coudert, F.-X. Structure, Dynamics, and Thermodynamics of Intruded Electrolytes in ZIF-8. *J. Phys. Chem. C* **2019**, *123*, 15589−15598.
(49) Chau, P.-L.; Hardwick, A. J. A New Order Parameter for Tetrahedral Configurations. *Mol. Phys.* **1998**, *93*, 511−518.
(50) Errington, J. R.; Debenedetti, P. Relationship Between Structural Order and the Anomalies of Liquid Water. *Nature* **2001**, *409*, 318−321.
(51) Duboué-Dijon, E.; Laage, D. Characterization of the Local Structure in Liquid Water by Various Order Parameters. *J. Phys. Chem. B* **2015**, *119*, 8406−8418.
(52) Rieth, A. J.; Hunter, K.; Dincă, M.; Paesani, F. Hydrogen bonding structure of confined water templated by a metal-organic framework with open metal sites. *Nat. Commun.* **2019**, *10*, No. 4771.
(53) Winkler, K.; Lindner, J.; Bürsing, H.; Vöhringer, P. Ultrafast Raman-induced Kerr-effect of water: Single molecule versus collective motions. *J. Chem. Phys.* **2000**, *113*, 4674.
(54) Lawrence, C. P.; Skinner, J. L. Vibrational spectroscopy of HOD in liquid D_2O. III. Spectral diffusion, and hydrogen-bonding and rotational dynamics. *J. Chem. Phys.* **2003**, *118*, 264.
(55) Rezus, Y. L. A.; Bakker, H. J. On the orientational relaxation of HDO in liquid water. *J. Chem. Phys.* **2005**, *123*, No. 114502.
(56) Krynicki, K.; Green, C. D.; Sawyer, D. W. Pressure and temperature dependence of self-diffusion in water. *Faraday Discuss. Chem. Soc.* **1978**, *66*, 199−208.
(57) Ghorbanfekr, H.; Behler, J.; Peeters, F. M. Insights into Water Permeation through hBN Nanocapillaries by Ab Initio Machine Learning Molecular Dynamics Simulations. *J. Phys. Chem. Lett.* **2020**, *11*, 7363−7370.
(58) Lee, C.-Y.; McCammon, J. A.; Rossky, P. J. The structure of liquid water at an extended hydrophobic surface. *J. Chem. Phys.* **1984**, *80*, 4448−4455.
(59) Jiang, J.; Gao, Y.; Zhu, W.; Liu, Y.; Zhu, C.; Francisco, J. S.; Zeng, X. C. First-Principles Molecular Dynamics Simulations of the Spontaneous Freezing Transition of 2D Water in a Nanoslit. *J. Am. Chem. Soc.* **2021**, *143*, 8177−8183.
(60) Hamid, I.; Jalali, H.; Peeters, F. M.; Neek-Amal, M. Abnormal in-plane permittivity and ferroelectricity of confined water: From sub-nanometer channels to bulk. *J. Chem. Phys.* **2021**, *154*, 114503.

https://doi.org/10.1021/acs.jcim.3c01077
J. Chem. Inf. Model. 2023, 63, 7097−7106

(61) Chakraborty, S.; Kumar, H.; Dasgupta, C.; Maiti, P. K. Confined Water: Structure, Dynamics, and Thermodynamics. *Acc. Chem. Res.* **2017**, *50*, 2139−2146.
(62) Cerveny, S.; Mallamace, F.; Swenson, J.; Vogel, M.; Xu, L. Confined Water as Model of Supercooled Water. *Chem. Rev.* **2016**, *116*, 7608−7625.
(63) Muñoz-Santiburcio, D.; Marx, D. Confinement-Controlled Aqueous Chemistry within Nanometric Slit Pores. *Chem. Rev.* **2021**, *121*, 6293−6320.
(64) Ceriotti, M.; Fang, W.; Kusalik, P. G.; McKenzie, R. H.; Michaelides, A.; Morales, M. A.; Markland, T. E. Nuclear Quantum Effects in Water and Aqueous Systems: Experiment, Theory, and Current Challenges. *Chem. Rev.* **2016**, *116*, 7529−7550.
(65) Mei, H. S.; Tuckerman, M. E.; Sagnella, D. E.; Klein, M. L. Quantum Nuclear ab Initio Molecular Dynamics Study of Water Wires. *J. Phys. Chem. B* **1998**, *102*, 10446−10458.
(66) Cao, Z.; Peng, Y.; Yan, T.; Li, S.; Li, A.; Voth, G. A. Mechanism of Fast Proton Transport along One-Dimensional Water Chains Confined in Carbon Nanotubes. *J. Am. Chem. Soc.* **2010**, *132*, 11395−11397.
(67) Towns, J.; Cockerill, T.; Dahan, M.; Foster, I.; Gaither, K.; Grimshaw, A.; Hazlewood, V.; Lathrop, S.; Lifka, D.; Peterson, G. D.; Roskies, R.; Scott, J. R.; Wilkins-Diehr, N. XSEDE: Accelerating Scientific Discovery. *Comput. Sci. Eng.* **2014**, *16*, 62−74.

NOTE ADDED AFTER ASAP PUBLICATION

This paper was originally published ASAP on October 9, 2023. Due to a production error, the TOC graphic was reprocessed. The correct version reposted on October 9, 2023.

https://doi.org/10.1021/acs.jcim.3c01077
J. Chem. Inf. Model. 2023, 63, 7097−7106